EISENBERG, R. & IBERS, J. A. (1965). *Inorg. Chem.* **4**, 773–778.
ELDER, R. C. & TRKULA, M. (1974). *J. Am. Chem. Soc.* **96**, 2635.
GIRLING, R. L. & AMMA, E. L. (1976). *Acta Cryst.* B**32**, 2903–2904.
GOLIĆ, L. & SPEAKMAN, J. C. (1965). *J. Chem. Soc. A*, pp. 2530–2542.
GONSCHOREK, W. & KÜPPERS, H. (1975). *Acta Cryst.* B**31**, 1068–1072.
HAMILTON, W. C. (1959). *Acta Cryst.* **12**, 609–610.
HORNSTRA, J. & STUBBE, B. (1972). *Processing of Paper Tape Output of Single-Crystal Diffractometer PW* 1100. Philips NV, Eindhoven.
International Tables for X-ray Crystallography (1974). Vol. IV, Tables 2.2*B* and 2.3.1. Birmingham: Kynoch Press.
JOHNSON, C. K. (1976). *ORTEP* II. Report ORNL-5318. Oak Ridge National Laboratory, Tennessee.
KVICK, Å., KOETZLE, T. F., THOMAS, R. & TAKUSAGAWA, F. (1974). *J. Chem. Phys.* **60**, 3866–3874.
LEBEDINSKII, V. V. & NOVOZHENYUK, Z. M. (1951). *Izv. Sekt. Platiny Drugikh Blagorodn. Met. Inst. Obshch. Neorg. Khim. Akad. Nauk SSSR*, **26**, 83–96.
MAIS, R. H. B., OWSTON, P. G. & WOOD, A. M. (1972). *Acta Cryst.* B**28**, 393–399.
MASLEN, E. N., RASTON, C. L. & WHITE, A. H. (1975). *J. Chem. Soc. Dalton Trans.* pp. 323–326.
MASLEN, E. N., RASTON, C. L., WHITE, A. H. & YANDELL, J. K. (1975). *J. Chem. Soc. Dalton Trans.* pp. 327–329.
MELANSON, R., HUBERT, J. & ROCHON, F. D. (1976). *Acta Cryst.* B**32**, 1914–1916.
MELANSON, R. & ROCHON, F. D. (1975). *Can. J. Chem.* **53**, 2371–2374.
MELANSON, R. & ROCHON, F. D. (1977). *Acta Cryst.* B**33**, 3571–3573.
MELANSON, R. & ROCHON, F. D. (1978*a*). *Acta Cryst.* B**34**, 941–943.
MELANSON, R. & ROCHON, F. D. (1978*b*). *Acta Cryst.* B**34**, 1125–1127.
MESSER, D., BREITINGER, D. K. & HAEGLER, W. (1979). *Acta Cryst.* B**35**, 815–818.
MESSER, D., BREITINGER, D. K. & HAEGLER, W. (1980). *Acta Cryst.* In the press.
MESSMER, G. G. & AMMA, E. L. (1966). *Inorg. Chem.* **5**, 1775–1781.
MESSMER, G. G., AMMA, E. L. & IBERS, J. A. (1967). *Inorg. Chem.* **6**, 725–730.
MILBURN, G. H. W. & TRUTER, M. R. (1966). *J. Chem. Soc. A*, pp. 1609–1616.
NEWMAN, G. & POWELL, D. B. (1963). *Spectrochim. Acta*, **19**, 213–224.
SHELDRICK, G. M. (1976). *SHELX* 76. Program for crystal structure determination. Univ. of Cambridge, England.
SHUBNIKOV, A. V. & KOPTSIK, V. A. (1974*a*). *Symmetry in Science and Art*, ch. 8, pp. 195–196. New York, London: Plenum.
SHUBNIKOV, A. V. & KOPTSIK, V. A. (1974*b*). *Symmetry in Science and Art*, ch. 9, p. 211. New York, London: Plenum.
SPINNLER, M. A. & BECKA, L. N. (1967). *J. Chem. Soc. A*, pp. 1194–1199.
WEBER, K. (1969). *Acta Cryst.* B**25**, 1174–1178.

Acta Cryst. (1980). B**36**, 2550–2554

A Study of the Ordered Structures of the Au–Mn System by High-Voltage–High-Resolution Electron Microscopy. I. Two-Dimensional Antiphase Structure of $Au_{31}Mn_9$ Based on the Au_4Mn Structure

BY K. HIRAGA, D. SHINDO AND M. HIRABAYASHI

The Research Institute for Iron, Steel and Other Metals, Tohoku University, Sendai, Japan

AND O. TERASAKI AND D. WATANABE

Department of Physics, Faculty of Science, Tohoku University, Sendai, Japan

(*Received* 6 *February* 1980; *accepted* 1 *July* 1980)

Abstract

A new two-dimensional antiphase structure, $Au_{31}Mn_9$, was determined directly from high-voltage–high-resolution electron microscopy on a Au–20·7 at.% Mn alloy. The space group is $P4/m$ and the unit cell is tetragonal having the lattice constants $A = \sqrt{10}a$ and $C = a$, where $a \simeq 4{\cdot}0$ Å is that of the fundamental f.c.c. cell. Satisfactory agreement can be obtained between the observed images and the calculations based on many-beam dynamical-diffraction theory. The proposed superstructure consists of square-shaped islands of the Au_4Mn structure of Ni_4Mo type containing 3×3 columns of manganese atoms; the islands are separated by two-dimensional antiphase boundaries parallel to the [310] and [$\bar{1}$30] directions of the fundamental f.c.c.

0567-7408/80/112550-05$01.00

lattice. The electron diffraction intensities calculated kinematically from the structure model agree well with the observed patterns.

I. Introduction

The crystal structure of Au–Mn alloys near Au_3Mn has been studied by many investigators using X-ray and electron diffraction techniques. They proposed the existence of several superstructures in the composition range 20–28 at.% Mn: *i.e.* Au_4Mn structure of the Ni_4Mo type (Watanabe, 1957); Au_3Mn structure sometimes called the Watanabe structure, which is characterized as the two-dimensional antiphase structure (2*d*-APS) based on the $L1_2$ type (Watanabe, 1960); and a series of structures derived from the DO_{22} type with long-period stacking order (Sato, Toth & Honjo, 1967). Recently, a model of 2*d*-APS which differs from the Watanabe structure was proposed by Tendeloo, Ridder & Amelinckx (1978) by means of 100 kV high-resolution electron microscopy using a dark-field technique. The structure consists of lozenge-shaped islands of the DO_{22} structure separated by antiphase boundaries (APB) of which the structure is related to the Au_4Mn structure. This structure was called a transition structure, since it was found by slow quenching or very short annealing after rapid quenching from the disordered state.

The appearance of these structures is known to depend quite sensitively upon composition and heat treatment, but the formation condition of these structures is still not clear. Therefore, we carried out a series of high-voltage–high-resolution electron microscopy (HVHREM) experiments to solve this problem. In the course of the experiments, we found a new 2*d*-APS, $Au_{31}Mn_9$. The present paper reports a direct determination of the atomic arrangement in this structure. Detailed studies on the existence range of various superstructures and the structure model of the 2*d*-APS derived from the high-resolution structure images will be reported in part II of the study.

II. Experiments

A specimen was prepared by melting appropriate amounts of Au and Mn with 99·99% purity in evacuated silica tubes. After heat treatment for homogenization at 1153 K for 17 h, the specimen was rolled into thin sheets. The sheets, sealed in evacuated silica capsules, were annealed at 673 K for 13 d for ordering, and were then quenched in water by breaking the tubes. The manganese content of the specimen was determined as 20·7 at.% by chemical analysis. Thin foils for electron microscopy were prepared by jet electropolishing using a solution of 30 ml hydrochloric acid, 30 ml sulphuric acid and 500 ml distilled water.

High-resolution observations were made with the Tohoku University 1 MV electron microscope (JEM 1000) which has a theoretical resolution of 1·9 Å. The objective aperture diameter was 70 μm. Direct magnification was 3×10^5 and exposure time was about 10 s. Astigmatism was corrected for by observing homogeneous granulation of contamination films adhering to the specimen edge. In order to avoid electron irradiation damage, the observations were made as quickly as possible.

III. Results and discussion

Fig. 1 shows a high-resolution electron micrograph of the Au–20·7 at.% Mn alloy. In the image, bright dots align regularly on a square lattice shown by white lines. The closest distance between the bright dots is 4·0 Å, and the lattice constant is 12·6 Å. The reverse-contrast image is shown in Fig. 2 of a neighboring region of Fig. 1. This fact indicates that the image contrast is sensitive to foil thickness. Details will be discussed later.

The above images are formed by a number of reflections up to the spacing $d \simeq 1{\cdot}9$ Å which corresponds to the 200 spot. The selected-area electron

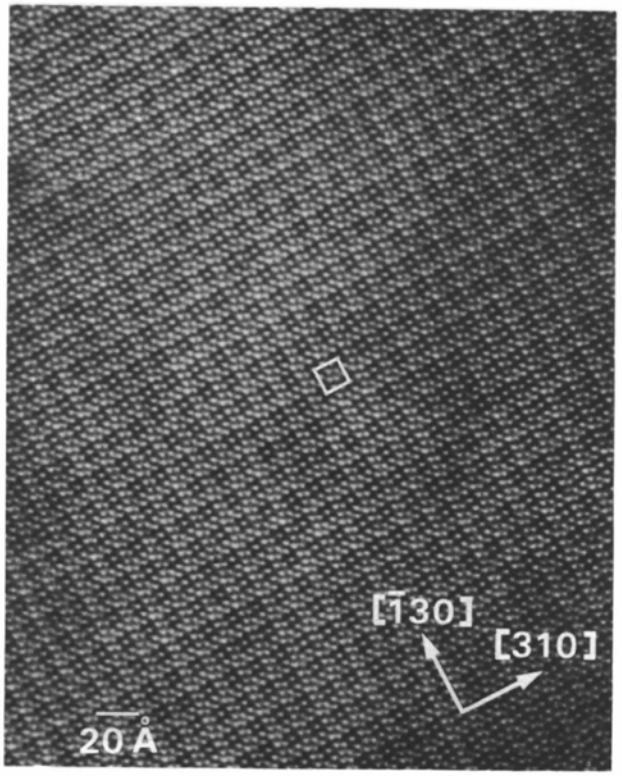

Fig. 1. High-resolution image of Au–20·7 at.% Mn alloy. One unit cell of $Au_{31}Mn_9$ is marked with a rectangle.

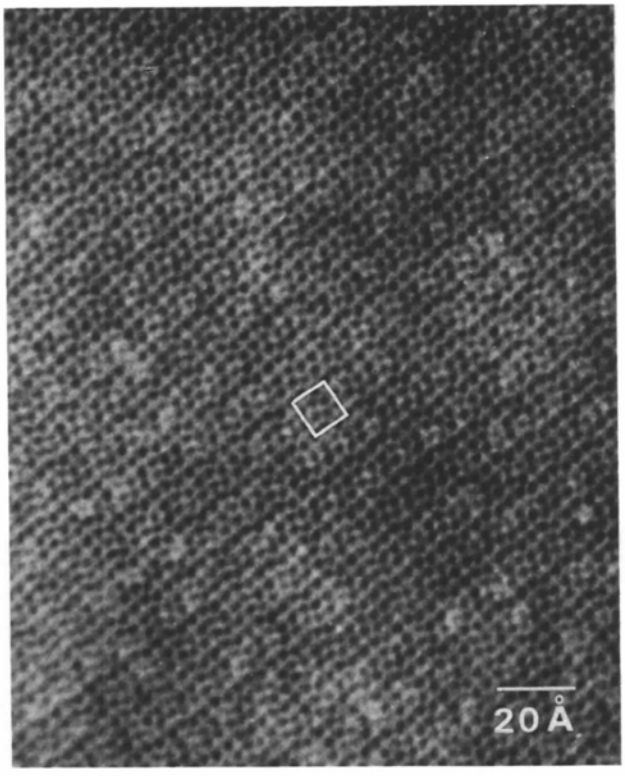

Fig. 2. High-resolution image of Au–20·7 at.% Mn alloy with reversed contrast.

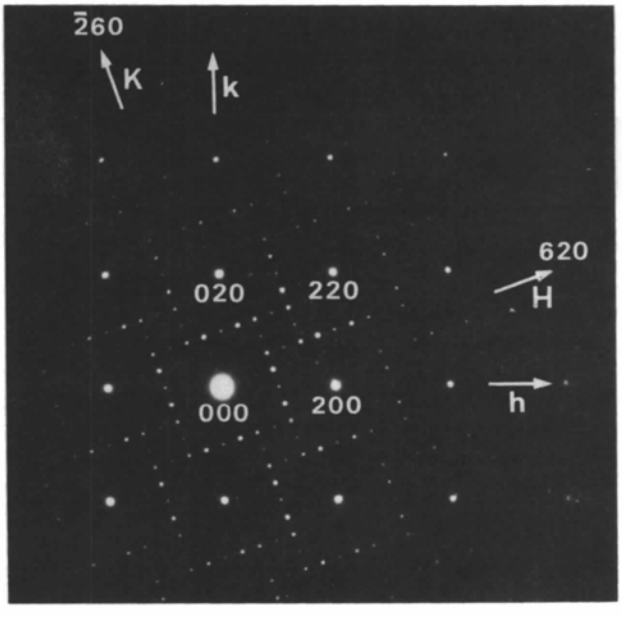

Fig. 3. Selected-area electron diffraction pattern of Au–20·7 at.% Mn alloy. The directions of **H**, **K**, **h** and **k** axes are shown by arrows.

diffraction pattern of Fig. 3 shows a characteristic distribution of superlattice spots, which are lying parallel to the lines connecting the origin and the 620 and $\bar{2}60$ spots with the periodic spacing of 1/20 of the reciprocal-lattice vectors for these two spots. Thus, the two orthogonal axes, **H** and **K**, for the superlattice may be taken parallel to these reciprocal-lattice vectors as illustrated in this pattern. The axes **H** and **K** are inclined at 19° to the original axes **h** and **k** of the fundamental f.c.c. lattice. The third axis, **L**, is perpendicular to the **HK** or **hk** plane, and no superperiod appears in this direction. From the diffraction patterns, the superlattice having a tetragonal cell with $A = \sqrt{10}a$ and $C = a$ is determined, where $a = 4{\cdot}0$ Å is the lattice constant of the fundamental f.c.c. structure. In the micrographs of Figs. 1 and 2, the incident beam is exactly parallel to the C axis, and the observed lattice constant 12·6 Å corresponds to $A = \sqrt{10}a$.

It seems rather difficult to determine the superstructure by analyzing the electron diffraction pattern, but an enlarged image of Fig. 4 allows us to propose directly a model for the new superstructure. If the bright dots are assumed to correspond to the Mn atom positions, we may immediately obtain the structure model illustrated in Fig. 5 which shows a projection of the atomic arrangement along the C axis. Note the one-to-one correspondence between the bright dots in the image and the Mn atom positions in the model. The closest Mn–Mn distance is $a = 4{\cdot}0$ Å. The tetragonal unit cell of the superstructure contains 40 atoms; 9 Mn and 31 Au.

To determine the atomic arrangements, it is important to compare the observed images with many-beam calculations based on dynamical-diffraction theory. We carried out the multislice calculation with the fast Fourier transform (Ishizuka & Uyeda, 1977) for the structure model of Fig. 5. The atomic positions in the $Au_{31}Mn_9$ structure are given in Table 1. Parameters used for the calculations are listed in Table 2. Fig. 6 shows the images calculated as a function of crystal thickness at the so-called optimum defocus condition (Scherzer, 1949). The image contrast changes appreci-

Table 1. *Superstructure of* $Au_{31}Mn_9$

Space group	$P4/m$ (No. 83), tetragonal
Unit-cell dimensions	$A = \sqrt{10}a = 12{\cdot}6$ Å, $C = a = 4{\cdot}0$ Å
Unit-cell contents	31 Au atoms, 9 Mn atoms
Atomic positions	
1 Mn in 1(a)	0,0,0
4 Mn in 4(j)	$x,y,0$; $\bar{x},\bar{y},0$; $\bar{y},x,0$; $y,\bar{x},0$
	$x = \frac{2}{5}, y = \frac{3}{10}$
4 Mn in 4(k)	$x,y,\frac{1}{2}$; $\bar{x},\bar{y},\frac{1}{2}$; $\bar{y},x,\frac{1}{2}$; $y,\bar{x},\frac{1}{2}$
	$x = \frac{1}{20}, y = \frac{7}{20}$
1 Au in 1(c)	$\frac{1}{2},\frac{1}{2},0$
2 Au in 2(e)	$0,\frac{1}{2},0$; $\frac{1}{2},0,0$
12 Au in 4(j)	$x = \frac{1}{10}, y = \frac{1}{5}$; $x = \frac{3}{10}, y = \frac{1}{10}$;
	$x = \frac{1}{5}, y = \frac{2}{5}$
16 Au in 4(k)	$x = \frac{3}{20}, y = \frac{1}{20}$; $x = \frac{1}{4}, y = \frac{1}{4}$;
	$x = \frac{9}{20}, y = \frac{3}{20}$; $x = \frac{7}{20}, y = \frac{9}{20}$

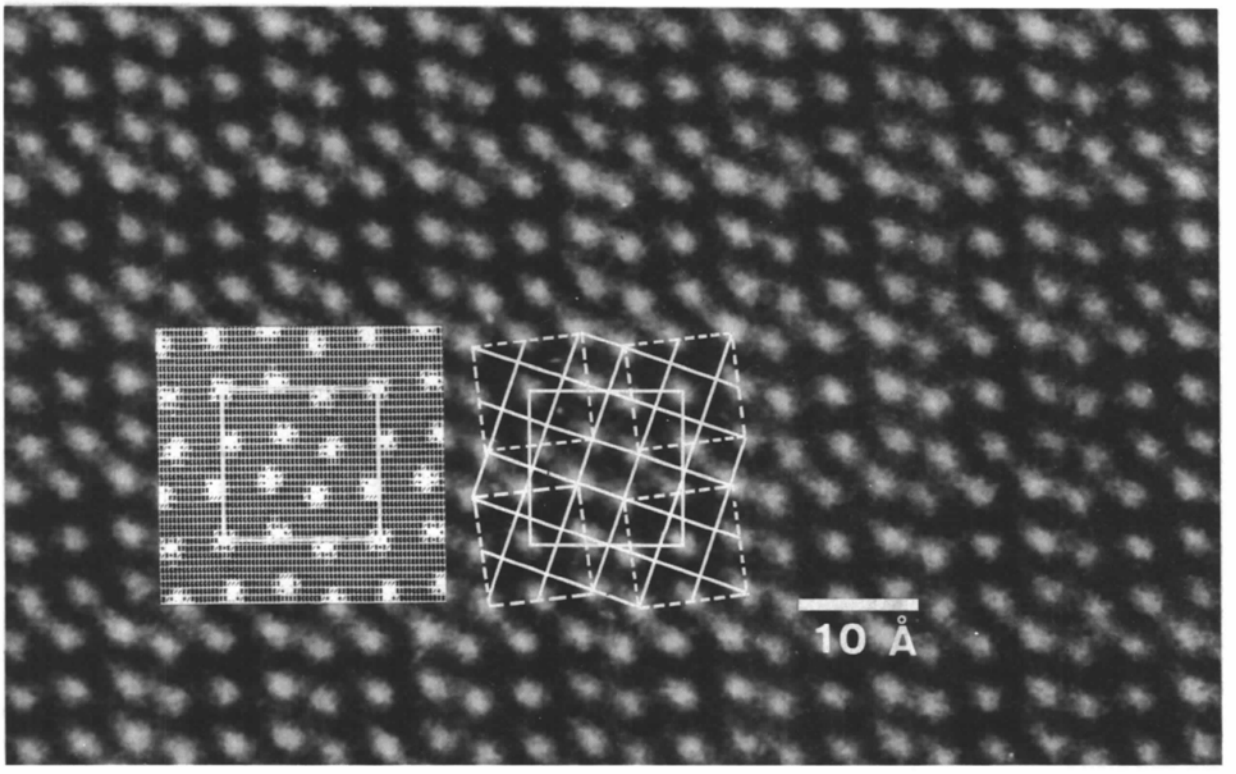

Fig. 4. Enlarged image of Fig. 1, showing the one-to-one correspondence between the bright dots and the Mn atom positions. The inset is a calculated image of the $Au_{31}Mn_9$ structure for thickness 160 Å.

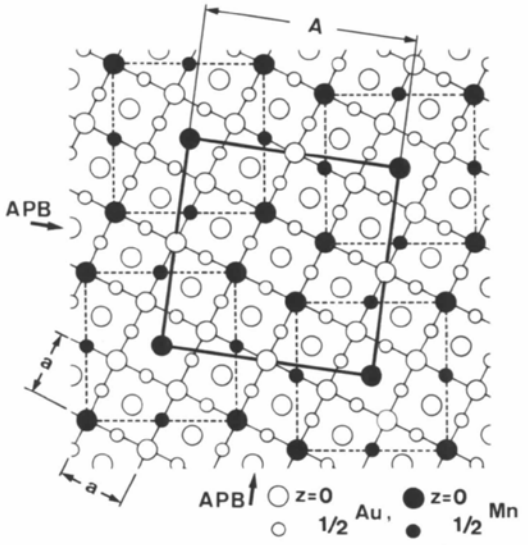

Fig. 5. Structure model of $Au_{31}Mn_9$. The islands of Au_4Mn structure are outlined by dotted lines.

ably with changing thickness; the calculations for 120 and 160 Å thickness reproduce well the observed images of Figs. 1 and 4. The image with the reversed contrast (Fig. 2) may correspond to the calculation corresponding to 280 and 320 Å. The calculation

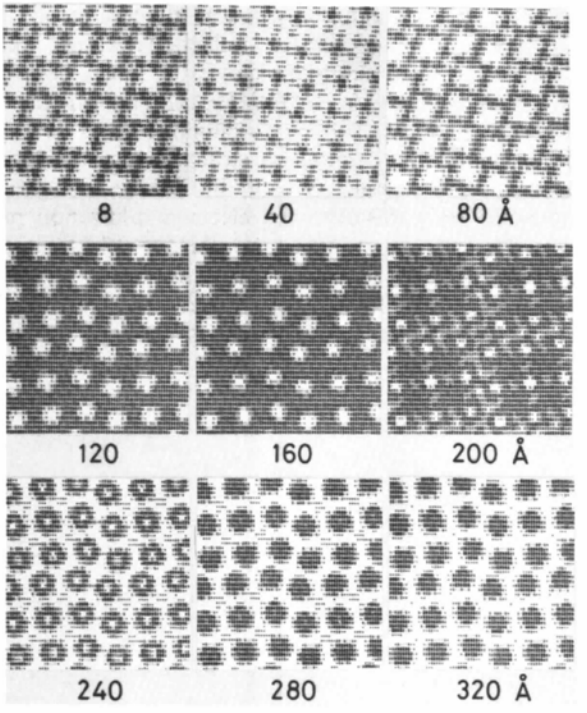

Fig. 6. Calculated images of the $Au_{31}Mn_9$ structure for thicknesses of 8–320 Å at $\Delta f = 1100$ Å.

Table 2. *Parameters used for image computation*

Accelerating voltage	1000 kV
Spherical aberration coefficient	11 mm
Defocus due to chromatic aberration	300 Å
Value of defocus	1100 Å
Objective aperture radius	0·55 $Å^{-1}$
Crystal thickness for one slice	8·0 Å
Number of beams	128 × 128

Table 3. *Calculated intensities of HK0 reflections of the* $Au_{31}Mn_9$ *structure*

*HK*0	*I*	*HK*0	*I*	*HK*0	*I*	*HK*0	*I*
010	<1	210	2	410	9	610	76
020	2	220	2	420	2	620	1
030	98	230	100	430	8	630	1
040	2	240	2	440	2	640	1
050	2	250	<1	450	<1	650	<1
060	2	260*	8699	460	1	660	1
070	<1	270	<1	470	<1	670	4
110	<1	310	44	510	39	710	14
120	<1	320	9	520	8	720	<1
130	22	330	43	530	35	730	<1
140	<1	340	2	540	71	740	<1
150	<1	350	<1	550	14	750	<1
160	<1	360	<1	560	56	760	<1
170	<1	370	<1	570	21	770	16

* This spot is the fundamental reflection 020 in terms of the indices of the basic f.c.c. structure.

indicates that the image contrast is affected mostly by the phases of superlattice reflections rather than fundamental ones. Some details of the image contrast have been discussed in our HVHREM work on Au–Cd alloys (Hirabayashi, Hiraga & Shindo, 1980).

To confirm the determined structure, the diffraction intensities are calculated from the above model and compared with the observed electron diffraction patterns. The calculated intensities of *HK*0 reflections are listed in Table 3, in which Doyle & Turner's (1968) atomic scattering factors of Au and Mn for electrons are used. Satisfactory agreement is obtained between the calculated and observed intensities of diffraction spots.

In the proposed model of Fig. 5, we note that the $Au_{31}Mn_9$ structure is composed of square-shaped islands of the Au_4Mn structure (Ni_4Mo type), which are separated by the 2*d*-APB parallel to the [310] and [$\bar{1}$30] directions. The atomic arrangement in the 2*d*-APB is isomorphic with that of the DO_{22} type.

The $Au_{31}Mn_9$ structure is found in the narrow composition range near 20·5 at.% Mn and coexists sometimes with the Au_4Mn structure. This is consistent with the fact that the Mn content of the $Au_{31}Mn_9$ structure (22·5 at.%) is slightly higher than that of the alloy examined. At higher Mn compositions, another type of 2*d*-APS appears, which is composed of parallelogram-shaped islands of the DO_{22} structure interconnected by the APB having an atomic arrangement isomorphic with that of the Au_4Mn structure. Detailed studies on the structure model of this 2*d*-APS and the existence range of various superstructures will be reported in part II of the study.

We would like to thank Mr H. Ota and Mr E. Aoyagi for their helpful collaboration throughout the work. The work has been partly supported by the Grant-in-Aid for Scientific Research from the Ministry of Education, Science and Culture.

References

Doyle, P. A. & Turner, P. S. (1968). *Acta Cryst.* A**24**, 390–397.

Hirabayashi, M., Hiraga, K. & Shindo, D. (1980). *J. Appl. Cryst.* To be published.

Ishizuka, K. & Uyeda, N. (1977). *Acta Cryst.* A**33**, 740–749.

Sato, H., Toth, R. S. & Honjo, G. (1967). *J. Phys. Chem. Solids*, **28**, 137–160.

Scherzer, O. (1949). *J. Appl. Phys.* **20**, 20–29.

Tendeloo, G. V., Ridder, R. D. & Amelinckx, S. (1978). *Phys. Status Solidi A*, **49**, 655–666.

Watanabe, D. (1957). *Acta Cryst.* **10**, 483–485.

Watanabe, D. (1960). *J. Phys. Soc. Jpn*, **15**, 1030–1040.